Int J Adv Manuf Technol (2018) 95:1607–1615
https://doi.org/10.1007/s00170-017-1243-8

ORIGINAL ARTICLE

Optimal cutting directions by considering the dynamic mismatch between feed axes of machine tools

Dun Lu[1] · Sanli Liu[1] · Xuewei Li[2] · Diaodiao Wu[1] · Wanhua Zhao[1] · Bingheng Lu[1]

Received: 14 March 2017 / Accepted: 24 October 2017 / Published online: 11 November 2017

Abstract Tool path generation is one of the key challenges in multi-axis sculptured surface machining. Besides geometry accuracy, machining processes have been considered in tool path generation in order to improve machining quality and efficiency as far as possible. However, so far, the machine tool accuracies have not been yet fully taken into account during tool path generation. Contour accuracy is one of the most important precision indexes to guarantee the machining quality of sculptured surfaces. One of the major reasons causing contour error is the dynamic mismatch between feed axes of machine tools. In this study, the mathematic relationship between the cutting direction, dynamic mismatch of feed axes and contour error is theoretically established. The mathematic relationship can be used to calculate the optimal cutting directions which minimize the contour error caused by dynamic mismatch between feed axes during machining a sculptured surface by a three-axis machine tool. A machining experiment is carried out to verify the mathematic relationship. In the experiment, the tool paths are generated along the optimal cutting direction and other cutting directions for comparison. The results show that the contour error under the case of the optimal cutting direction is much smaller than that under the other cases.

✉ Dun Lu
dunnlu@xjtu.edu.cn

[1] State Key Laboratory for Manufacturing Systems Engineering, Xi'an Jiaotong University, Xi'an 710054, China

[2] School of Mechanical Engineering, Shandong University of Technology, Zibo, Shandong 255012, China

Keywords Optimal cutting direction · Tool paths generation · Sculptured surface · Contour error · Following error · Dynamic mismatch

1 Introduction

Tool path generation is one of the key challenges in sculptured surface machining with multi-axis machine tools. The classical methods of tool path generation, including iso-parametric, iso-planar, and iso-scallop methods, etc., mainly focus on geometry accuracy of parts by restraining scallop heights. Iso-parametric methods [1–4] generate tool paths for a parametric surface, in which a parameter increases with an interval and other parameters stay the same. The interval must be changed for satisfying scallop height when the curvature of the parametric surface changes. Iso-planar methods [5–8] use curves intersected by a series of isometric planes and the machining surface as tool paths. The plane distances are determined by scallop height. Iso-scallop methods [9–11] select an initial tool path in machining surface and generate the tool paths through retaining scallop heights to constant.

Besides geometry accuracy, machining processes and machine tool accuracies have also been considered in tool path generation in order to improve machining quality and efficiency [12].

In machining processes, tool paths represent cutting directions of tool relative to machining surface; therefore, it has significant effects on cutting width, material removal rate, and tool deformation. Marcinial [13] and Kruth [14] investigated the relationship between the cutting width and the cutting directions. They found that the maximum cutting width was acquired when the cutting directions matched the principal curvature direction of the part surface. Chiou [15] proposed a Machine Potential Field approach which maximizes

the cutting width and minimizes the path length by optimizing the cutting directions. Kim [16] developed a greedy approach to search the optimal cutting directions for maximizing material removal rate. In this approach, the optimal cutting directions were represented as a vector field. The tool paths can be modeled as streamlines of the vector field. Giri and Bezbaruah [17] divided the part surface into different regions according to the curvature to shorten the machining time. The initial tool paths were selected along the direction of the maximum or the minimum curvature in each region, while the adjacent paths were determined by iso-scallop method. Lim [18] investigated the effects of cutting directions on the tool deformation. The tool deformations caused by the cutting forces under different cutting directions were calculated. The optimal cutting directions were found based on the maximum feed rate as well as the minimum tool deformation.

Dynamic accuracies of machine tools are seriously dependent on tool paths. Non-smooth tool paths lead to the discontinuity of acceleration/deceleration, and then cause the vibrations of feed axes of machine tools. Erkorkmaz [19] presented a quintic spline tool path generation algorithm that produced continuous position, velocity, and acceleration profiles. Held [20] introduced an algorithm for generating a G^1-continuous spiral tool path for high-speed machining. Li [21] presented a method for generating tool paths with smooth tool motion based on the Accessibility Map. Zheng [22] proposed a method to smooth the tool path with a constraint on the geometric error. In order to obtain the smoother feed, acceleration, and jerk profiles along the tool path, Yuen [23] developed a spline interpolation method in which the tool tip and orientation locations generated by the CAM system were first fitted to B-spline. Ernesto [24] developed a method to modify the commanded path for a given federate. By this method, the physical trajectory conformed more closely to the original commanded path. Rahaman [25] introduced a robust following controller that merges a cross-coupled controller with real-time federate modification. Kim [26] presented a precise approach to generate tool paths of collision free and gouging free. To achieve high approximation quality, the approach combines Hyper-osculating Circles and two-contact configurations. Bo [27] introduced a method that approximates free-form surfaces by envelopes of one-parameter motions of surfaces of revolution.

As mentioned above, the machining processes and machine tools performance should be considered in tool paths generation for achieving high accuracy and high speed machining. However, so far, the machine tools accuracies have not been yet fully taken into account.

Contour accuracy is one of the most important precision indexes of machine tools to guarantee the machining quality of sculptured surfaces. Usually, contour accuracy is controlled by reducing following errors of feed axes of machine tools after tool paths generation. Following error is a kind of dynamic errors of machine tools which relate with feed rates. Due to flexibility [28, 29] and limitation of the bandwidth of feed axes [30], following errors cannot be substantially reduced. Coordinating following errors by matching dynamics of feed axes to guarantee contour accuracy has become an inevitable tendency [31]. Poo [32], Xi [33], and Yeh [34] developed gain-matching order dynamic matching methods to coordinate the following errors of each axes, and consequently reduced the contour errors during two- or three-axis machining. Lei [35], Lin [36], and Jiang [37] investigated dynamic matching methods for five-axis machine tools based on the contour error of given test curves and parts. Although the works mentioned above were successfully achieved the gains and dynamic match at some specific cases, dynamics between feed axes usually cannot be matched due to different mechanical dynamics. Dynamic mismatch between feed axes may lead to mis-coordinate of following errors, and hence contour errors.

It is noted that following errors are dynamic errors which relate with feed rates. Coincidentally, feed rates of each feed axes can be changed by means of adjusting direction of tool path (i.e., the cutting direction), relative to feed axes in machine tools. Therefore the aim of this study is to establish the mathematic relationship between cutting direction, dynamic mismatch and contour error, and then carried out an experiment to verify the feasibility to generate tool path with optimal cutting directions for reducing contour error caused by dynamic mismatch. Three-axis machine tools have relatively simpler kinematic configurations than five-axis machine tools. It is easier for three-axis machine tools to calculate the contour error from the three following errors. Therefore, in this study, only the kinematic configuration of three-axis machine tools is considered to investigate the mathematic relationship.

2 Mathematic relationship between cutting direction, dynamic mismatch, and contour error

The procedure that a CAD model of a sculptured part is machined into a physical part is as follows: firstly, a CAD model is converted into tool paths and G codes by CAM; then, the G codes are interpolated into position commands (velocity commands); finally, the position commands are used as inputs of feed axes to achieve the feed motion, as shown in Fig. 1. Due to the inertia effects, the actual positions of feed axes are usually lagged behind the command positions. The difference between the command and actual positions are following errors which result in contour error in machining sculptured surfaces with multi-axis machine tools. Therefore, the mathematic expression of following error should be established primarily.

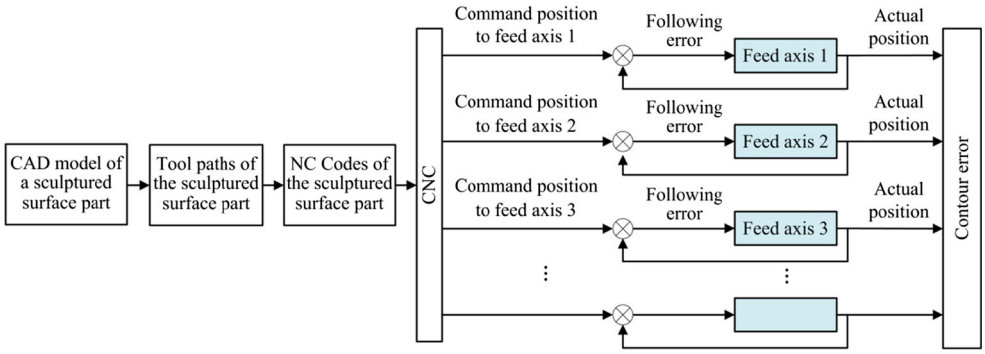

Fig. 1 The procedure that a CAD model of a sculptured part is machined into a physical part

2.1 Mathematic expression of following error

A typical feed axis of a machine tool is usually simplified as a second-order model [30, 33], as shown in Fig. 2.

The transfer function of the second order model can be expressed as:

$$G(s) = \frac{\omega_n^2}{s^2 + 2\zeta\omega_n s + \omega_n^2} \tag{1}$$

where ω_n is undamped natural frequency and ζ is viscous ratio.

The viscous ratio ζ is usually a little bit less than 1 for rapidity of feed motions in machine tools, so the unit step response of the feed axis can be expressed as:

$$h(t) = 1 - \frac{e^{-\zeta\omega_n t}}{\sqrt{1-\zeta^2}} \sin\left(\omega_n\sqrt{1-\zeta^2}t + \arctan\frac{\sqrt{1-\zeta^2}}{\zeta}\right) \tag{2}$$

Set the command position of the feed axis (the input of the feed axis) as $x_c(t)$. It can be regarded as the superposition of a series of unit step commands. So, the output of the feed axis (actual position) can be expressed as:

$$x_o(nT) = \sum_{k=1}^{n} \{x_c(kT) - x_c[(k-1)T]\} h(nT-kT) \tag{3}$$

When the time interval T is small enough,the actual position at time t can be rewritten as:

$$\begin{aligned} x_o(t) &= \int_{-\infty}^{t} x_c'(\tau) h(t-\tau)\mathrm{d}\tau \\ &= \int_{-\infty}^{t} x_c'(\tau)\mathrm{d}\tau - \int_{-\infty}^{t} x_c'(\tau) \frac{e^{-\zeta\omega_n(t-\tau)}}{\sqrt{1-\zeta^2}} \sin\left[\omega_n\sqrt{1-\zeta^2}(t-\tau) + \arctan\frac{\sqrt{1-\zeta^2}}{\zeta}\right]\mathrm{d}\tau \\ &= x_c(t) - \int_{-\infty}^{t} x_c'(\tau) \frac{e^{-\zeta\omega_n(t-\tau)}}{\sqrt{1-\zeta^2}} \sin\left[\omega_n\sqrt{1-\zeta^2}(t-\tau) + \arctan\frac{\sqrt{1-\zeta^2}}{\zeta}\right]\mathrm{d}\tau \end{aligned} \tag{4}$$

Set

$$\eta(t) = \frac{e^{-\zeta\omega_n t}}{\sqrt{1-\zeta^2}} \sin\left(\omega_n\sqrt{1-\zeta^2}t + \arctan\frac{\sqrt{1-\zeta^2}}{\zeta}\right) \tag{5}$$

The following error $e(t)$ is the difference between the command position and actual position,

$$e(t) = x_c(t) - x_o(t) = \int_{-\infty}^{t} x_c'(\tau)\eta(t-\tau)\mathrm{d}\tau \tag{6}$$

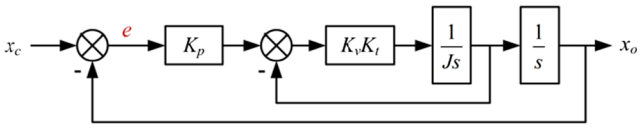

Fig. 2 Equivalent block diagram of a feed axis in machine tools

If the command position is derivable, in the neighborhood at time t_0, the command position can be written as:

$$\begin{aligned} x_c(t) = x_c(t_0) &+ x_c'(t_0)(t-t_0) + \frac{1}{2}x_c''(t_0)(t-t_0)^2 \\ &+ \frac{1}{6}x_c'''(t_0)(t-t_0)^3 \cdots \\ &+ \frac{1}{n!}x_c^n(t_0)(t-t_0)^n + \frac{1}{(n+1)!}x_c^{n+1}(t_0)\xi^{n+1} \end{aligned} \tag{7}$$

Substituting Eq. (7) into Eq. (6), truncating the infinitesimal item of $e^{-\zeta\omega_n t}$, the expression of following error can be rewritten as:

$$e(t) = x_c'(t)\frac{2\zeta}{\omega_n} - x_c''(t)\frac{4\zeta^2-1}{\omega_n^2} + x_c'''(t)\frac{8\zeta^3-4\zeta}{\omega_n^3} + \cdots \tag{8}$$

For feed axes in machine tools, $\omega_n \gg 1 \approx \zeta$, therefore,

$$\frac{2\zeta}{\omega_n} \gg \frac{4\zeta^2-1}{\omega_n^2} \gg \frac{8\zeta^3-4\zeta}{\omega_n^3} \gg \cdots \tag{9}$$

And because $x'(t) = v(t)$,

Equation (8) can be rewritten as:

$$e(t) \approx v(t)\frac{2\zeta}{\omega_n} \tag{10}$$

The viscous ratio ζ and the undamped natural frequency ω_n of second-order systems can be expressed as:

$$\begin{cases} \zeta = \dfrac{1}{2}\sqrt{\dfrac{K_v K_t}{JK_p}} \\ \omega_n = \sqrt{\dfrac{K_p K_v K_t}{J}} \end{cases} \tag{11}$$

where K_p is the gain of position loop, K_v is the gain of velocity loop, K_t is the torque constant of motor, and J is the rotary inertia of motor rotor.

Substituting Eq. (11) into Eq. (10), the following error can be finally expressed as:

$$e(t) \approx 2\frac{v(t)}{K_p} \tag{12}$$

2.2 Geometrical relationships between following errors of feed axes and contour errors

It can be seen from Eq. (12) that the following error *e(t)* of a feed axis is the function of the feed rate *v(t)* and the dynamic parameters K_p of the feed axis. It is noted that the feed rate *v(t)* of each axis is assigned by the interpolator of CNC. The programming feed rate in G codes and the directions of tool path (cutting directions) decide the feed rate *v(t)* of each axis. In addition, for multi-axis machine tools, each feed axis has different dynamic parameters. Therefore, the mathematic relationship between cutting direction, dynamic mismatch and contour error can be established by analyzing the geometric relationship between contour errors and following errors.

The geometrical relationships between following errors of feed axes of a three-axis machine tool and contour errors are shown in Fig. 3. In this figure, the machine tool's coordinate is compose of three components of *X*, *Y*, and *Z* which represent the feed directions of the *X*-, *Y*-, and *Z*-axis, respectively. The blue curve is on a sculptured surface which is transformed from the work-piece coordinate to the machine tools coordinate. P_c represents a point on the sculptured surface. *V* is the programming feed rate at P_c point. The direction of *V* is the cutting direction at P_c point. A, B, and C are included angles between the cutting direction and the *X*-, *Y*-, and *Z*-axis of the machine tool, respectively. v_x, v_y, and v_z interpolated by the CNC of the machine tool are the command velocities (command positions) of the *X*-, *Y*-, and *Z*-axis.

It is assumed that the actual position is on point P_a when the command position locates on point P_c, because the actual positions always lag behind the command positions. The difference between the command position and the actual position is defined as the following error $\boldsymbol{E}$. Its components along *X*, *Y*, and *Z* directions, i.e., the following errors of *X*-, *Y*-, and *Z*-axis are e_x, e_y, and e_z, respectively.According to Eq. (12), the following errors e_x, e_y, and e_z of *X*-, *Y*-, and *Z*-axis can be expressed as:

$$\begin{aligned} \mathbf{E}(t) &= \left[e_x(t), e_y(t), e_z(t)\right] \\ &= \left[\frac{2}{K_{px}}v_x(t), \frac{2}{K_{py}}v_y(t), \frac{2}{K_{pz}}v_z(t)\right] \end{aligned} \tag{13}$$

The following errors of e_x, e_y, and e_z result in a deviation between the actual point P_a and the sculptured surface. The minimum distance between the actual point P_a and the sculptured surface is defined as contour error $\varepsilon(t)$. According to the geometrical relationship, the contour error $\varepsilon(t)$ can be expressed as:

$$\begin{aligned} \varepsilon(t) &= \boldsymbol{\alpha} \times \mathbf{E} \times \boldsymbol{\alpha} \\ &= V(t)\begin{bmatrix} \cos A\left(\delta_{xz}\cos^2 C - \delta_{yx}\cos^2 B\right) \\ \cos B\left(\delta_{yx}\cos^2 A - \delta_{zy}\cos^2 C\right) \\ \cos C\left(\delta_{zy}\cos^2 B - \delta_{xz}\cos^2 A\right) \end{bmatrix}^T \end{aligned} \tag{14}$$

where $\boldsymbol{\alpha} = (\cos A, \cos B, \cos C)^T$

2.3 Function expression reflecting the relationship of cutting direction, dynamic mismatch, and contour error

According to Eq. (14), the magnitude of contour error $|\varepsilon|$ can be expressed as:

$$|\varepsilon(t)| = V(t)\sqrt{\delta_{xz}\cos^2 A\cos^2 C + \delta_{yx}\cos^2 A\cos^2 B + \delta_{zy}\cos^2 B\cos^2 C} \tag{15}$$

$$\begin{cases} \delta_{xz} = 2\left(\dfrac{1}{K_{px}} - \dfrac{1}{K_{pz}}\right) \\ \delta_{yx} = 2\left(\dfrac{1}{K_{py}} - \dfrac{1}{K_{px}}\right) \\ \delta_{zy} = 2\left(\dfrac{1}{K_{pz}} - \dfrac{1}{K_{py}}\right) \end{cases} \tag{16}$$

Equation (15) shows that the magnitude of contour error $|\varepsilon|$ depends on the programming feed rate *V*, the dynamic mismatch δ_{xz}, δ_{yx}, and δ_{zy} between axes of machine tools, and the included angles A, B, and C. It can be seen from Eq. (15) that the programming feed rate *V* and the magnitude of contour error $|\varepsilon|$ have

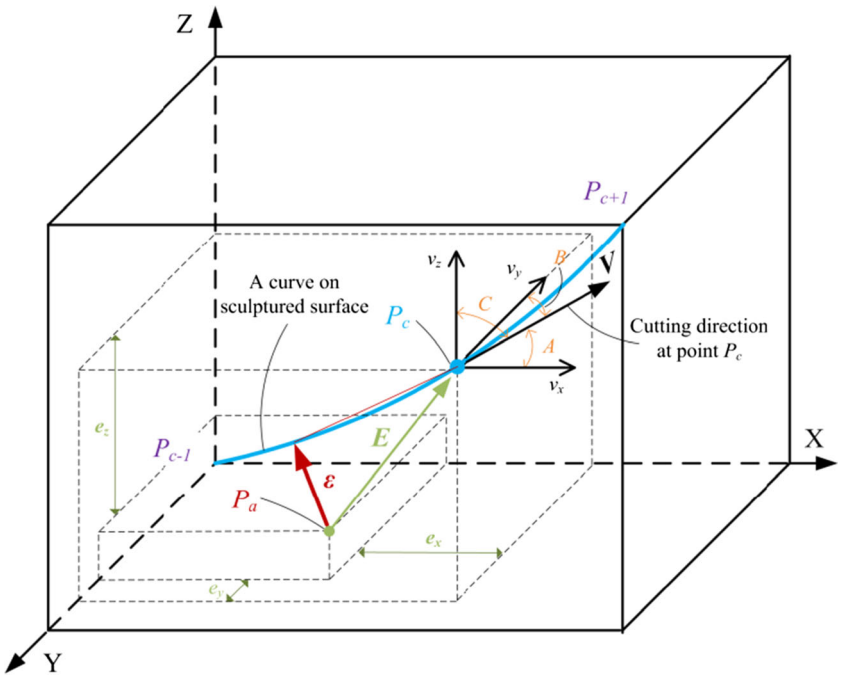

Fig. 3 The geometrical relationship between following errors and contour errors

positive correlation. Therefore, some methods including feed rate scheduling [38] and look-ahead [39] have been developed in order to reduce contour error by optimizing programming feed rates. Δ_{xz}, δ_{yx}, and δ_{zy} represent the dynamic mismatch between the three axes. When the dynamics between feed axes match, i.e., the position gains of each axis are the same, δ_{xz}, δ_{yx}, and δ_{zy} equal to zero, then the contour error can be completely eliminated. Otherwise, when the dynamic mismatch, i.e., δ_{xz}, δ_{yx}, and δ_{zy} are not zero, the included angles A, B, and C are the only remaining variables which can be capably regulate the contour error. The included angles A, B, and C just represent the cutting direction in the machine tool's coordinate.

To sum up, Eq. (15) can be regarded as a mathematic model which constructs the relationship between cutting direction of sculptured surface parts, dynamic performance of machine tools, and accuracy of machine tools. It establishes the theoretical basis

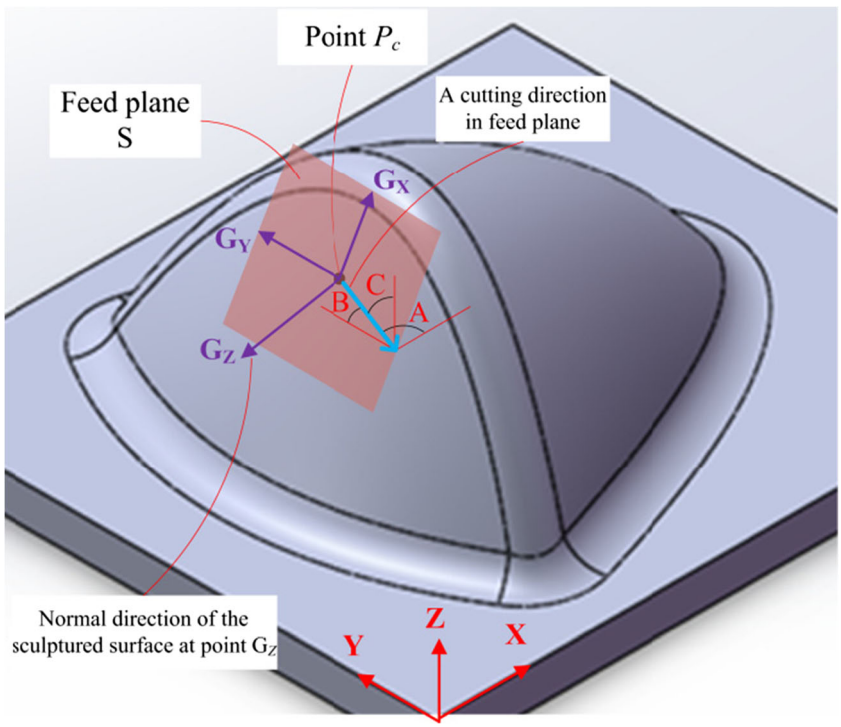

Fig. 4 Feed plane *S* and cutting direction at point P_c on a sculptured surface

Table 1 Three cases of dynamic mismatch for a three-axis machine tool

Cases of dynamic mismatch of a 3-axis machine tool	I	II	III
Undamped natural frequencies	$\omega_{nx} = \omega_{ny} = \omega_{nz} = 60$ rad/s		
Viscous ratios	$\zeta_x = 0.79, \zeta_y = 0.73, \zeta_z = 0.76$	$\zeta_x = 0.73, \zeta_y = 0.76, \zeta_z = 0.79$	$\zeta_x = 0.75, \zeta_y = 0.79, \zeta_z = 0.73$
Gains of position loop	$K_x = 75.9, K_y = 82.2, K_z = 78.9$	$K_x = 82.2, K_y = 78.9, K_z = 75.9$	$K_x = 80, K_y = 75.9, K_z = 82.2$
Parameters of dynamic mismatch	$\delta_{xz} = 1.00 \times 10^{-3}$ $\delta_{yx} = 2.20 \times 10^{-3}$ $\delta_{zy} = 1.02 \times 10^{-3}$	$\delta_{xz} = -2.02 \times 10^{-3}$ $\delta_{yx} = 1.02 \times 10^{-3}$ $\delta_{zy} = 1.00 \times 10^{-3}$	$\delta_{xz} = 6.69 \times 10^{-4}$ $\delta_{yx} = 1.35 \times 10^{-3}$ $\delta_{zy} = -1.01 \times 10^{-3}$

of the optimum cutting direction based on the dynamic mismatch between feed axes to minimize the contour error.

3 Solving method for the optimal cutting directions

A simple sculptured surface part is designed to illustrate the solving method of the optimal cutting directions, as shown in Fig. 4. The coordinate of the part *X*, *Y*, and *Z* are set along the *X*-, *Y*- and *Z*- axis of a three-axis milling machine tool. It is assumed that there is a point P_c on the sculptured surface. Construct a feed plane *S* which goes through the point P_c and is tangent to the sculptured surface at point P_c. G_Z is the normal direction of the feed plane *S*. G_X and G_Y are in the plane *S*. The direction of G_Y is parallel to the plane *XY*.

Because the cutting direction at the point P_c should be tangent to the sculptured surface, the cutting direction must be in plane *S*. A, B, and C are the included angles between the cutting direction and *X*-, *Y*-, and *Z*-axis, respectively. When the cutting direction rotates around point P_c in the feed plane *S*, the included angles A, B, and C should be changed. Accordingly, the contour error should be changed with the A, B, and C. The A, B, and C at which the contour error researches the minimum are selected as the optimal cutting direction at point P_c.

In order to illustrate the effects of dynamic mismatch on optimal cutting directions, the contour errors under the three cases of dynamic mismatch are calculated by Eq. (15). The three cases of dynamic mismatch are set by keeping the undamped natural frequencies ω_n constant but changing the viscous ratios ζ for a three-axis machine tool, as shown in Table 1.

The contour error trajectories under the three cases of dynamic mismatch are shown in Fig. 5. It can be seen from this figure that the contour errors vary with the cutting directions, which means different cutting direction has different contour error. Since variables A, B, and C contained in Eq. (15) are all the forms of "$\cos^2$," the contour errors at opposite cutting directions have the same magnitude. The cutting directions at which the contour errors reach the minimum are selected as the optimal cutting direction at point P_c. Obviously, when the tool paths are generated along the optimal cutting directions, the contour error can be minimized even though the feed axes have dynamic mismatch.

Furthermore, it can be seen from Fig. 5a–c that the optimal cutting direction change according to the dynamic mismatch between the feed axes. It means that there is a special cutting direction corresponding to a special dynamic mismatch. Different dynamic mismatches between feed axes should generate different optimal cutting directions.

4 Experimental verification

4.1 Experimental method

A three-axis milling machine tool with dynamic mismatch is selected to carry out the experiments. When the feed

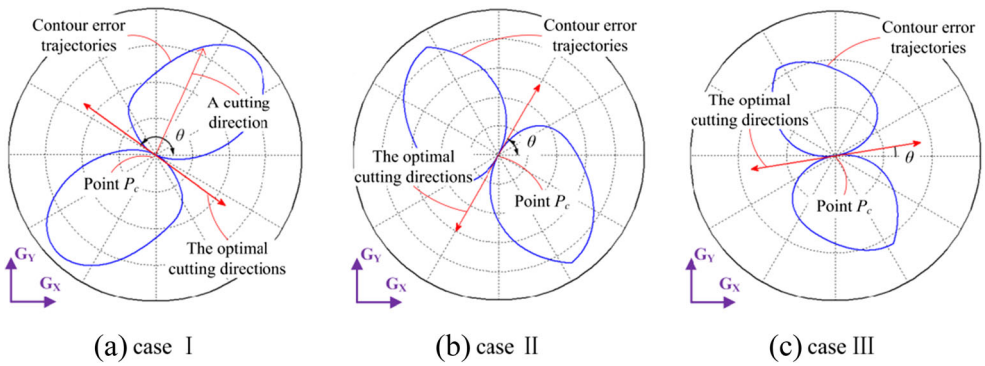

Fig. 5 The optimal cutting directions under three cases of dynamic mismatch

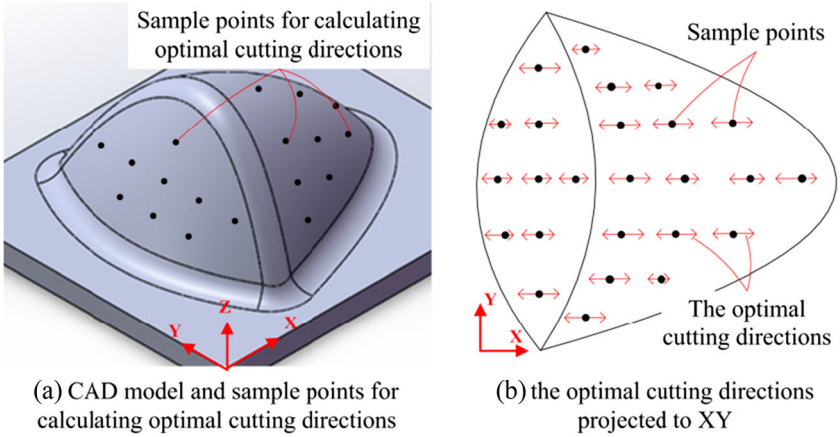

Fig. 6 **a**, **b** The experimental sculptured surface part and its optimal cutting directions

(a) CAD model and sample points for calculating optimal cutting directions

(b) the optimal cutting directions projected to XY

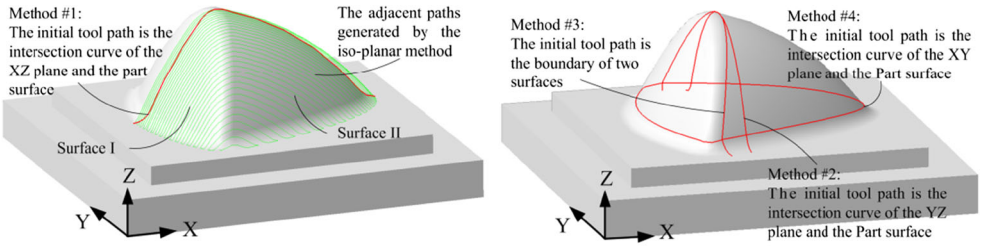

Fig. 7 **a**, **b** The tool paths for the experimental sculptured surface part

(a) the tool paths along the optimal cutting directions

(b) the tool paths for comparison

rate is 1 m/min, the following errors of the three axes e_x, e_y, and e_z are 0.32, 0.21, and 0.34 mm, respectively. According to Eqs. (13) and (16), the parameters of dynamic mismatches δ_{xz}, δ_{yx}, and δ_{zy} for the experimental machine tool are 2.4×10^{-3} s, -1.3×10^{-2} s, and 1.6×10^{-2} s, respectively.

Besides the dynamic mismatching machine tool, the sculptured surface part as shown in Fig. 3 is employed as the experimental part. The length, width, and height of the part are 65.8, 64.5, and 28.3 mm, respectively. Twenty-five sample points distributed on the part surface are selected for determining the optimal cutting directions on the

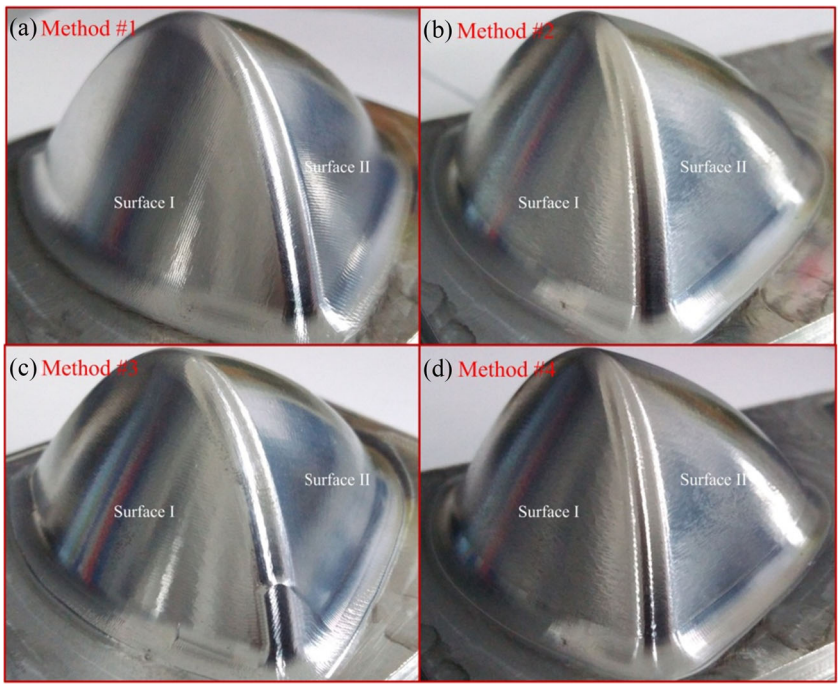

Fig. 8 Photos of experimental parts after machining

Table 2 The contour error of the part in different cutting directions

Method No.	Surface I/mm	Surface II/mm	Length of tool path/mm
1	0.038	0.042	30,901
2	0.127	0.183	35,765
3	0.104	0.153	26,042
4	0.128	0.188	27,569

different positions, as shown in Fig. 6a. The optimal cutting directions are calculated by the method mentioned in Section 3. The optimal cutting directions at all sample points are projected to *XY* plane of workpiece coordinate for better visualization, as shown in Fig. 6b. It can be seen that the optimal cutting directions are all perpendicular to the *Y* direction and tangent to the part surface.

The tool paths are generated along the optimal cutting directions and other directions for machining of the sculptured surface part. Because all the optimal cutting directions are in *XZ* plane, an intersection curve of the *XZ* plane and part surface is selected as the initial tool path. The adjacent tool paths are generated by iso-planar method with the limited scallop height of 0.16 μm, as shown in Fig. 7a. Thus the tool paths can meet the requirement of the optimal cutting directions as well as the geometry accuracy. For comparison, the initial tool paths are also set to the intersection line of *YZ* plane and the surface, the intersection line of *XY* plane, and the surface and the boundary of two surfaces, as shown in Fig. 7b.

The ball-end tool of φ8 mm is used to machine the sculptured surface part. The feed rate is 2 m/min. The speed of spindle is 8000 r/min. The depth of cut is 0.1 mm. And the material of the part is aluminum alloy 7075.

4.2 Contour accuracy under different cutting directions

The four tool paths are employed to machine the sculptured surface part. The photos after machining are shown in Fig. 8. The contour accuracies are measured by a Coordinate Measuring Machine with an accuracy of 0.001 mm.

As shown in Table 2, the average contour error of surface I of methods 2, 3, and 4 is 0.120 mm, and that of surface II is 0.175 mm, while the contour errors of surfaces I and II of method 1 are 0.038 and 0.042 mm, respectively. The reduction ratios are 68 and 76%, respectively.

The cutting directions of 1 are perpendicular to the *Y*-axis, therefore the item of cos*B* in Eq. (15) is zero. In the same way, because the cutting directions of 2 and 4 are perpendicular to the *X*- and *Z*-axis, respectively, the item of cos*A* and cos*C* in Eq. (15) are zero. According to Eq. (15), the contour error of 1, 2, and 4 can be simplified as:

$$\begin{cases} |\varepsilon(t)|_1 = v(t)\sqrt{\delta_{xz}\cos^2 A\cos^2 C} \\ |\varepsilon(t)|_2 = v(t)\sqrt{\delta_{zy}\cos^2 B\cos^2 C} \\ |\varepsilon(t)|_4 = v(t)\sqrt{\delta_{yx}\cos^2 A\cos^2 B} \end{cases} \tag{17}$$

The cutting directions of 3 are not perpendicular to the three axes of the machine tool, so the contour error of 3 should be calculated by Eq. (15).

The contour errors are determined by the dynamic mismatch of δ_{xz}, δ_{yx}, and δ_{zy} and the cutting directions A, B, and C. Because the δ_{xz} is much smaller than the δ_{yx} and δ_{zy} for the experimental machine tool, the contour error of 1 is smaller than that of 2 and 4. In addition, the δ_{yx} and δ_{zy} are similar but opposite in sign, which reduce the contour error caused by δ_{yx} and δ_{zy}. So, the contour error of 3 is larger than that of 1 and smaller than that of 2 and 4.

5 Conclusions

1) The mathematic relationship between cutting direction, dynamic mismatch of feed axes, and contour error is established in this study. According to the dynamic mismatch of a three-axis machine tool, the optimal cutting directions can be determined for minimizing contour error.
2) It is feasible in theory that the tool paths can be generated along the optimal cutting directions for reducing the contour error caused by dynamic mismatch between feed axes.

Funding information This work is financially supported by the project of the National Natural Science Funds of China (Grant No. 51775421), the Major Project of High-end CNC Machine Tool and Basic Manufacturing Equipment of China (Grant No. 2015ZX04001002), and the Project funded by China Postdoctoral Science Foundation (Grant No. 2015M570824).

References

1. Loney GC, Ozsoy TM (1987) NC machining of free form surfaces. Comput Aided Des 19(2):85–90
2. Bobrow James E (1985) NC machine tool path generation from CSG part representations. Comput Aided Des 17(2):69–75
3. Elber G, Cohen E (1994) Toolpath generation for freeform surface models. Comput Aided Des 26(6):490–496
4. Lo CC (2000) CNC machine tools surface interpolator for ball-end milling of free-form surfaces. Int J Mach Tool Manu 40(3):307–326
5. Huang Y, Oliver JH (1994) Non-constant parameter NC tool path generation on sculptured surfaces. Int J Adv Manuf Technol 9(5): 281–290

6. Park SC, Choi BK (2000) Tool-path planning for direction-parallel area milling. Comput Aided Des 32(1):17–25
7. Sarma SE (2000) The crossing function and its application to zig-zag tool paths. Comput Aided Des 31(4):881–890
8. Lartigue C, Thiebaut F, Maekawa T (2001) CNC tool path in terms of B-spline curves. Comput Aided Des 33(4):307–309
9. Suresh K, Yang DCH (1994) Constant scallop-height machining of free-form surfaces. Journal of Engineering for Industry 116:253–259
10. Lo CC (1999) Efficient cutter-path planning for five-axis surface machining with a flat-end cutter. Comput Aided Des 31:557–566
11. Lee YS (1998) Non-isoparametric tool path planning by machining strip evaluation for 5-axis sculptured surface machining. Comput Aided Des 30(7):559–570
12. Harik RF, Gong H, Bernard A (2013) 5-axis flank milling: a state-of-the-art review. Comput Aided Des 45:796–808
13. Marciniak K (1987) Influence of surface shape on admissible tool positions in 5-axis face milling. Comput Aided Des 19(5):233–236
14. Kruth JP, Klewais P (1994) Optimization and dynamic adaptation of the cutter inclination during five-axis milling of sculptured surfaces. CRIP Annals-Manufacturing Technology 43(1):443–448
15. Chiou CJ, Lee YS (2002) A machining potential field approach to tool path generation for multi-axis sculptured surface machining. Comput Aided Des 34(5):357–371
16. Kim T, Sarma SE (2002) Tool path generation along directions of maximum kinematic performance; a first cut at machine-optimal paths. Comput Aided Des 34(6):453–468
17. Giri V, Bezbaruah D, Bubna P, Choudhury AR (2005) Selection of master cutter paths in sculptured surface machining by employing curvature principle. Int J Mach Tool Manu 45(10):1202–1209
18. Lim EM, Menq CH (1997) Integrated planning for precision machining of complex surfaces. Part 1: cutting-path and feedrate optimization. Int J Mach Tool Manu 37(1):61–75
19. Erkorkmaz K, Altintas Y (2001) High speed CNC system degisn. Part 1: jerk limited trajectory generation and quintic spline interpolation. Int J Mach Tool Manu 41:1323–1345
20. Held M, Spielberger C (2009) A smooth spiral tool path for high speed machining of 2D pockets. Comput Aided Des 41:539–550
21. Li LL, Zhang YF, Li HY, Geng L (2011) Generating tool-path with smooth posture change for five-axis sculptured surface machining based on cutter's accessibility map. Int J Adv Manuf Technol 53: 699–709
22. Zheng G, Bi QZ, Zhu LM (2012) Smooth tool path generation for five-axis flank milling using multi-objective programming. Proc Inst Mech Eng B J Eng Manuf 226:247–254
23. Yuen A, Zhang K, Altintas Y (2013) Smooth trajectory generation for five-axis machine tools. Int J Mach Tools Manuf 71:11–19
24. Ernesto CA, Farouki RT (2010) Solution of inverse dynamics problems for contour error minimization in CNC machines. Int J Adv Manuf Technol 49(5-8):589–604
25. Rahaman M, Seethaler R, Yellowley I (2015) A new approach to contour error control in high speed machining. Int J Mach Tools Manuf 88:42–50
26. Kim Y-J, Elber G, Bartoň M, Pottmann H (2015) Precise gouging-free tool orientations for 5-axis CNC machining. Comput Aided Des 58:220–229
27. Bo PB, Bartoň M, Plakhotnik D, Pottmann H (2016) Towards efficient 5-axis flank CNC machining of free-form surfaces via fitting envelopes of surfaces of revolution. Comput Aided Des 79:1–11
28. Li BT, Hong J, Liu ZF (2014) Stiffness design of machine tool structures by a biologically inspired topology optimization method. Int J Mach Tools Manuf 84(2):33–44
29. Gao XM, Li BT, Hong J, Guo JK (2016) Stiffness modeling of machine tools based on machining space analysis. Int J Adv Manuf Technol 86(5–8):2093–2106
30. Altintas Y, Verl A, Brecher C, Uriarte L, Pritschow G (2011) Machine tool feed drives. CIRP Annals-Manufacturing Technology 60:779–796
31. Huo F, Poo AN (2013) Precision contouring control of machine tools. International Journal of Advance Manufacture Technology 64:319–333
32. Poo AN, Bollinger JG, Younkin GW (1972) Dynamic errors in type 1 contouring systems. IEEE Transaction on Industry Applications IA-8(4):477–484
33. Xi XC, Poo AN, Hong GS (2009) Improving contouring accuracy by tuning gains for a bi-axial CNC machine. Int J Mach Tool Manu 49:395–460
34. Yeh SS, Hsu PL (2004) Perfectly matched feedback control and its integrated design for multi-axis motion system. Journal of Dynamic System Measure and Control 126(3):547–557
35. Lei WT, Paung IM, CC Y (2009) Total ballbar dynamic tests for five axis CNC machine tools. Int J Mach Tool Manu 49:488–499
36. Lin MT, SK W (2013) Modeling and analysis of servo dynamics errors on measuring paths of five axis machine tools. Int J Mach Tool Manu 66:1–14
37. Jiang Z, Ding JX, Song ZY (2016) Modeling and simulation of surface morphology abnormality of S test piece machined by five axis CNC machine tool. International Journal of Advance Manufacture and Technology 85:2745–2759
38. Sencer B, Altintas Y, Croft E (2008) Feed optimization for five-axis CNC machine tools with drive constraints. Int J Mach Tool Manu 48:733–745
39. Jin YA, He Y, JZ F (2013) A look-ahead and adaptive speed control algorithm for parametric interpolation. International Journal of Advanced Manufacture Technology 69:2613–2620